LETTERS
https://doi.org/10.1038/s41565-018-0186-z
nature nanotechnology

Electric-field control of magnetism in a few-layered van der Waals ferromagnetic semiconductor

Zhi Wang[1,2,11], Tongyao Zhang[3,4,11], Mei Ding[5,11], Baojuan Dong[1,2,11], Yanxu Li[3,4], Maolin Chen[1,2], Xiaoxi Li[1,2], Jianqi Huang[1,2], Hanwen Wang[1,2], Xiaotian Zhao[1,2], Yong Li[1,2], Da Li[1,2], Chuankun Jia[5], Lidong Sun[6], Huaihong Guo[7], Yu Ye[8,9], Dongming Sun[1,2], Yuansen Chen[3,4]*, Teng Yang[1,2]*, Jing Zhang[3,4], Shimpei Ono[10], Zheng Han[1,2]* and Zhidong Zhang[1,2]

Manipulating a quantum state via electrostatic gating has been of great importance for many model systems in nanoelectronics. Until now, however, controlling the electron spins or, more specifically, the magnetism of a system by electric-field tuning has proven challenging[1–4]. Recently, atomically thin magnetic semiconductors have attracted significant attention due to their emerging new physical phenomena[5–13]. However, many issues are yet to be resolved to convincingly demonstrate gate-controllable magnetism in these two-dimensional materials. Here, we show that, via electrostatic gating, a strong field effect can be observed in devices based on few-layered ferromagnetic semiconducting $Cr_2Ge_2Te_6$. At different gate doping, micro-area Kerr measurements in the studied devices demonstrate bipolar tunable magnetization loops below the Curie temperature, which is tentatively attributed to the moment rebalance in the spin-polarized band structure. Our findings of electric-field-controlled magnetism in van der Waals magnets show possibilities for potential applications in new-generation magnetic memory storage, sensors and spintronics.

Though most van der Waals (vdW) magnets behave as semiconductors, very few reports have been conducted on field-effect transistors (FETs) based on such magnets[3,4]. In particular, studies that utilize an electric field to effectively tune their magnetism are lacking. So far, multiple approaches have been developed, including multiferroic heterostructures[14], thin metals[15–17], multilayered magnetic thin films[18–20] and diluted magnetic semiconductors[21,22]. In this Letter we show that few-layered semiconducting $Cr_2Ge_2Te_6$ devices can remain conducting and gate-tunable below their ferromagnetic Curie temperature. Micro-area Kerr measurements at low temperatures were carried out on $Cr_2Ge_2Te_6$ transistors with both ionic liquid and solid Si gates, which enabled tunable magnetization loops at different gate doping.

Single-crystal $Cr_2Ge_2Te_6$ was prepared using the Te self-flux method and confirmed by X-ray diffraction (see Methods and Supplementary Fig. 1), then further fabricated (see Methods) into a FET (Fig. 1a). An atomic force microscope (AFM) scan of typical flakes is shown in Fig. 1b,c. Before measuring few-layered $Cr_2Ge_2Te_6$, we obtained zero-field-cooled (ZFC) and field-cooled (FC) thermal magnetization curves of its bulk. As shown in Fig. 1d, the Curie temperature is determined to be around 64 K with a 1,000 G magnetic field applied perpendicular to the *a*–*b* plane of the bulk crystal (Supplementary Fig. 2).

For a $Cr_2Ge_2Te_6$ FET with thickness t of ~19 nm and source–drain voltage of $V_{ds}=2$ V, a source–drain current I_{ds} on the order of a few μA is obtained. I_{ds} as a function of temperature is recorded in Fig. 1e with a constant V_{ds} of 2 V. It is seen that I_{ds} drastically decreases on lowering the temperature, logarithmically following a T^{-4} law (Supplementary Fig. 3). Moreover, the I–V characteristics of the devices show an ohmic to semiconducting transition on lowering the temperature, as shown in Supplementary Fig. 4. This behaviour is typical of a semiconductor, and is in agreement with previous reports[4,7]. We found that the $Cr_2Ge_2Te_6$ device with thickness of 10 nm turned into an insulator below 150 K (Supplementary Fig. 5), which is much higher than its Curie temperature (T_C). A systematic study of such devices in air (Supplementary Figs. 6–8) indicated a clear drop in I_{ds} and enhanced gate tunability with decreasing layer thickness, as summarized in Fig. 1f.

The magneto-optic Kerr effect has been widely used in surface science, including the recent 2D vdW magnetic materials[4–7]. Here, we use an ultrahigh-sensitivity Kerr set-up with a low-temperature vacuum cryostat to investigate the magnetization of few-layered $Cr_2Ge_2Te_6$ transistors, while monitoring their electrical transport in situ. An optical diagram and the measuring protocols are described in Supplementary Fig. 9. By using an objective close to the sample surface, a spot size with a diameter of about 2 μm was achieved with the incident laser with a wavelength of 800 nm. Supplementary Fig. 10a presents micro-area Kerr measurements at different temperatures for a $Cr_2Ge_2Te_6$ device (thickness of about 19 nm). At $T=70$ K the sample behaves paramagnetically, in good

[1]Shenyang National Laboratory for Materials Science, Institute of Metal Research, Chinese Academy of Sciences, Shenyang, China. [2]School of Material Science and Engineering, University of Science and Technology of China, Anhui, China. [3]State Key Laboratory of Quantum Optics and Quantum Optics Devices, Institute of Opto-Electronics, Shanxi University, Taiyuan, China. [4]Collaborative Innovation Center of Extreme Optics, Shanxi University, Taiyuan, China. [5]College of Materials Science and Engineering, Changsha University of Science & Technology, Changsha, China. [6]State Key Laboratory of Mechanical Transmission, School of Materials Science and Engineering, Chongqing University, Chongqing, China. [7]College of Sciences, Liaoning Shihua University, Fushun, China. [8]State Key Lab for Mesoscopic Physics and School of Physics, Peking University, Beijing, China. [9]Collaborative Innovation Center of Quantum Matter, Beijing, China. [10]Central Research Institute of Electric Power Industry (CRIEPI), Materials Science Research Laboratory, Yokosuka, Kanagawa, Japan. [11]These authors contributed equally: Zhi Wang, Tongyao Zhang, Mei Ding, Baojuan Dong. *e-mail: yuansen.chen@sxu.edu.cn; yangteng@imr.ac.cn; hanzheng@imr.ac.cn

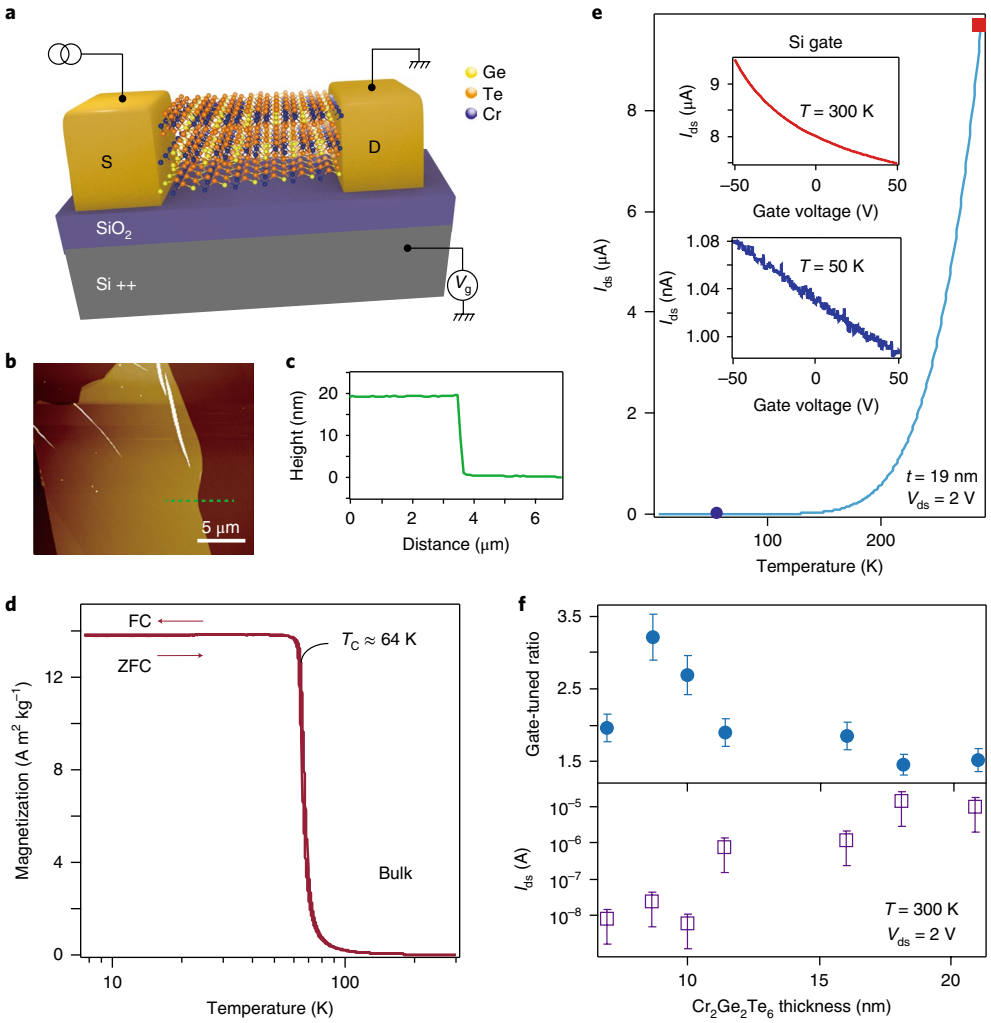

Fig. 1 | Characterization of $Cr_2Ge_2Te_6$ and its FET with a Si gate. a, Schematic of Au-contacted few-layered $Cr_2Ge_2Te_6$ device. **b**, AFM image of a typical $Cr_2Ge_2Te_6$ flake of ~19 nm in thickness. **c**, Height profile of the flake along the green dashed line in **b**. **d**, Magnetization of bulk $Cr_2Ge_2Te_6$ as a function of temperature with ZFC and FC processes. **e**, I_{ds} as a function of temperature for a typical 19 nm $Cr_2Ge_2Te_6$ device, with $V_{ds}=2$ V and $V_g=-50$ V. Insets: field-effect curves at 300 K (top) and 50 K (bottom), respectively. Red and blue inset curves correspond to positions shown as solid squares and circles in the I_{ds}–T curve. **f**, A statistic on $Cr_2Ge_2Te_6$ FET devices with different layer thickness at room temperature. Top, gate-tuned ratio calculated from the ratio of I_{ds} at $V_g=-50$ V and +50 V. Bottom, I_{ds} at $V_g=0$ V. All measurements were performed with $V_{ds}=2$ V.

agreement with the ZFC–FC characterization of its bulk form. On decreasing the temperature below 60 K, it shows ferromagnetic loops, with an enhanced saturation field at lower temperature (Supplementary Fig. 11). However, even with the largest possible gate voltages (from −80 V to +70 V, with total charge doping on the order of 10^{13} cm^{-2}; ref. [23]) applied on the $Cr_2Ge_2Te_6$ transistors, no obvious tuning of the Kerr signal was observed at $T<T_C$, as shown in Supplementary Fig. 10b.

Ionic liquids such as N,N-diethyl-N-methyl-N-(2-methoxyethyl) ammonium bis(trifluoromethylsulfonyl)imide (DEME-TFSI) are often used for gate-tuning of semiconductor conducting channels because the molecules in the liquid can form an electric double layer (EDL) that significantly reduces the thickness compared to conventional solid dielectric materials[24,25]. Figure 2a shows a schematic image of a $Cr_2Ge_2Te_6$ flake on a Si/SiO_2 substrate contacted by Cr/Au (5/50 nm) electrodes. Together with the contacts, a large-area pad acting as a gate was defined close to the sample. A small droplet of DEME-TFSI was placed onto the device and the gate pad, followed by a glass cap that covered the whole area, enabling access for the laser for further Kerr measurements. Before cooling, the device was left in vacuum at room temperature at a pressure of ~1×10^{-4} mbar for a few hours. It was then cooled to 235 K (above the freezing point of DEME-TFSI[25]) to test the field-effect curves.

As shown in Fig. 2b, within a chemical window of ±4 V (for more details see Supplementary Fig. 12), the sample is stable and a strong field effect can be obtained, with a gate-tuned ratio of about 10 (defined as the ratio of I_{ds} for gate voltage $V_g=-4$ V and +4 V). The I–V characteristics show a linear behaviour at all gate voltages at 235 K, as shown in Supplementary Fig. 13. Note that the field-effect curve stabilizes after several thermal cycles (Supplementary Fig. 14) as there is a surface potential reconfiguration process that takes place until a stable state is reached. Once the field-effect curve is stabilized, the sample was cooled below T_C for Kerr measurements. Figure 2c shows I–V characteristics of the same device with fixed ionic gate voltages of 0, −2 and −4 V, respectively, measured at 20 K. A semiconducting output curve is seen at low temperature, but with a much higher I_{ds} than obtained in the Si-gated devices for similar $Cr_2Ge_2Te_6$ flake thickness.

Strikingly, unlike the Si-gated $Cr_2Ge_2Te_6$ FETs (Supplementary Fig. 10b), a renormalized magnetization loop of the devices gated

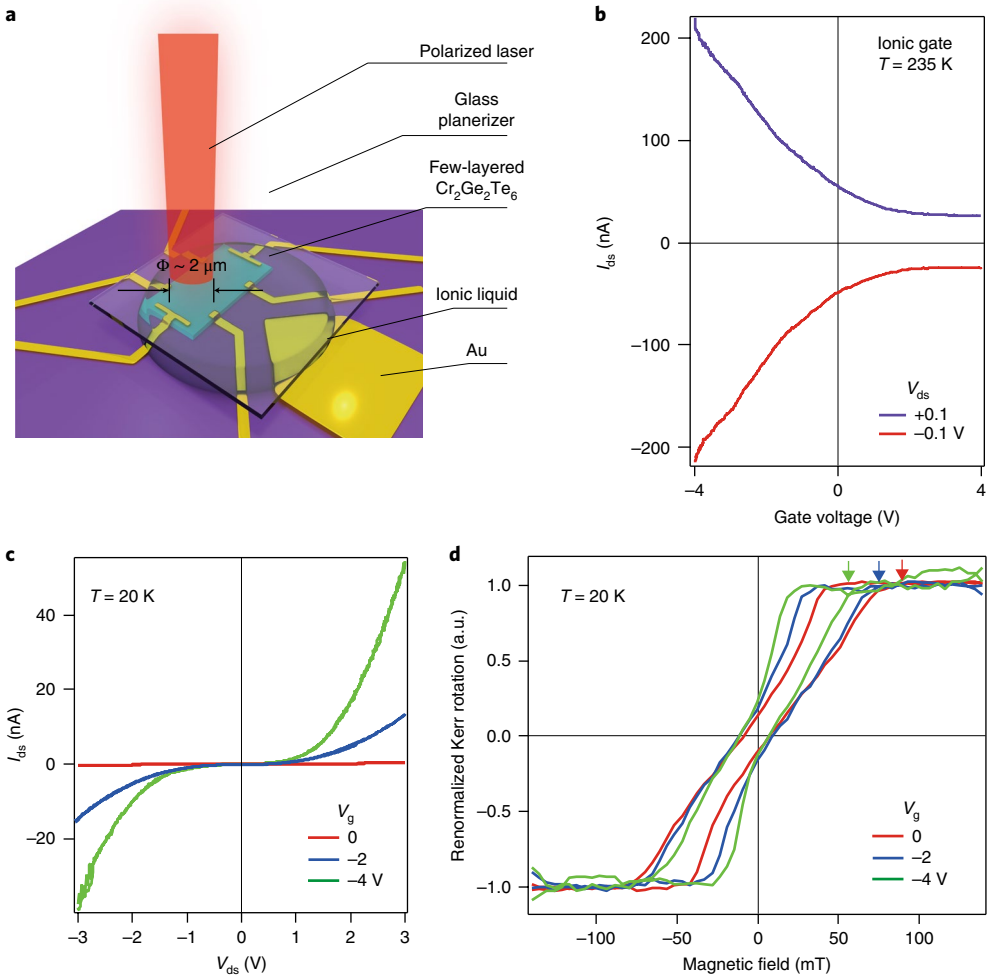

Fig. 2 | Electrical transport and magnetic properties of ~20 nm $Cr_2Ge_2Te_6$ FETs with ionic gate. a, Schematic image of the experimental set-up for Kerr measurement of the micrometre-sized device using ionic liquid. **b**, Field-effect curves at 235 K with $V_{ds} = -0.1$ and +0.1 V, respectively. **c**, *I*–*V* characteristics of the same device with fixed ionic gate voltages of 0, −2 and −4 V, measured at 20 K. **d**, Renormalized Kerr angle measured at 20 K and with fixed ionic gate voltages of 0, −2 and −4 V. Coloured arrows indicate H_s for the loops measured at each V_g. Note that the ionic liquid freezes below 220 K, so the curves are taken for several different cooling procedures.

by ionic liquid can be largely tuned, as shown in Fig. 2d. If we take the $V_g = -4$ V loop, for example, the saturation field H_s, indicated by arrows in Fig. 2d, can be reduced by a factor of 2 at $V_g = -4$ V compared to the values of the loop measured at $V_g = 0$ V. For the ionic liquid DEME-TFSI used here, the gate-induced carrier density n_{2D} is usually about 100 times higher than that in solid-state FETs with 285 nm oxides[25]. We also studied the magnetic domain of bulk $Cr_2Ge_2Te_6$, as shown in Supplementary Fig. 15. It is seen that the domain sizes are less than 2 μm (as reported elsewhere[26]), smaller than the laser spot used in the Kerr measurements. We also measured multiple samples and verified the reproducibility of the experiment, as shown in Supplementary Figs. 16 and 17.

To push the $Cr_2Ge_2Te_6$ into a true 2D limit, we assembled samples with much reduced thickness using a state-of-the-art BN encapsulation technique in a glove box[7–9], as shown in Fig. 3a–d. Thanks to the enhanced air stability, BN-encapsulated $Cr_2Ge_2Te_6$ with 3.5 nm thickness demonstrates the field effect as well as semiconducting characteristics, even below the Curie temperature, as shown in Fig. 3e. Note that the electrically probed gap becomes larger on lowering the temperature, along a source–drain current with reduced amplitude . Interestingly, as shown in Fig. 3f, the sample shows transport on both the electron and hole sides, exhibiting the behaviour of a bipolar FET. This allows the investigation of gate doping for both conduction and valence bands.

As shown in Fig. 4a,b, when cooled to 40 K, the sample shows a source–drain current of tens of nA with typical p-type semiconducting *I*–*V* and field-effect curves. However, the fact that n-type transport is missing at this low temperature may be due to a contact issue (or the gate needs to be more positive), as is often seen in semiconducting vdW materials. Strikingly, at this temperature, the Si gate can effectively tune the hysteresis loop with both electron and hole doping, as illustrated by the Kerr measurements in Fig. 4c,d.

In both ionic and Si-gated samples (thick and thin), the hole doping effects on the magnetic loop of $Cr_2Ge_2Te_6$ are consistent. With hole doping, an enhanced saturation magnetization (M_s) and a reduced saturation field (H_s), as well as a doping-insensitive coercivity (H_c), are observed, as shown in Figs. 2d and 4c,d. In fact, for relatively thicker samples ($t \sim 20$ nm), there is indeed always a gradient of the electric field and the $Cr_2Ge_2Te_6$ layers are no exception. The carriers induced by the ionic liquid are often active in the top layers, but are screened deeper in the sample in the *z* direction. Moreover, due to the highly resistive nature of the samples, we failed to extract the exact value of carrier density via Hall measurements, so, in the scenario of ionic gating, the hole number per unit (carrier

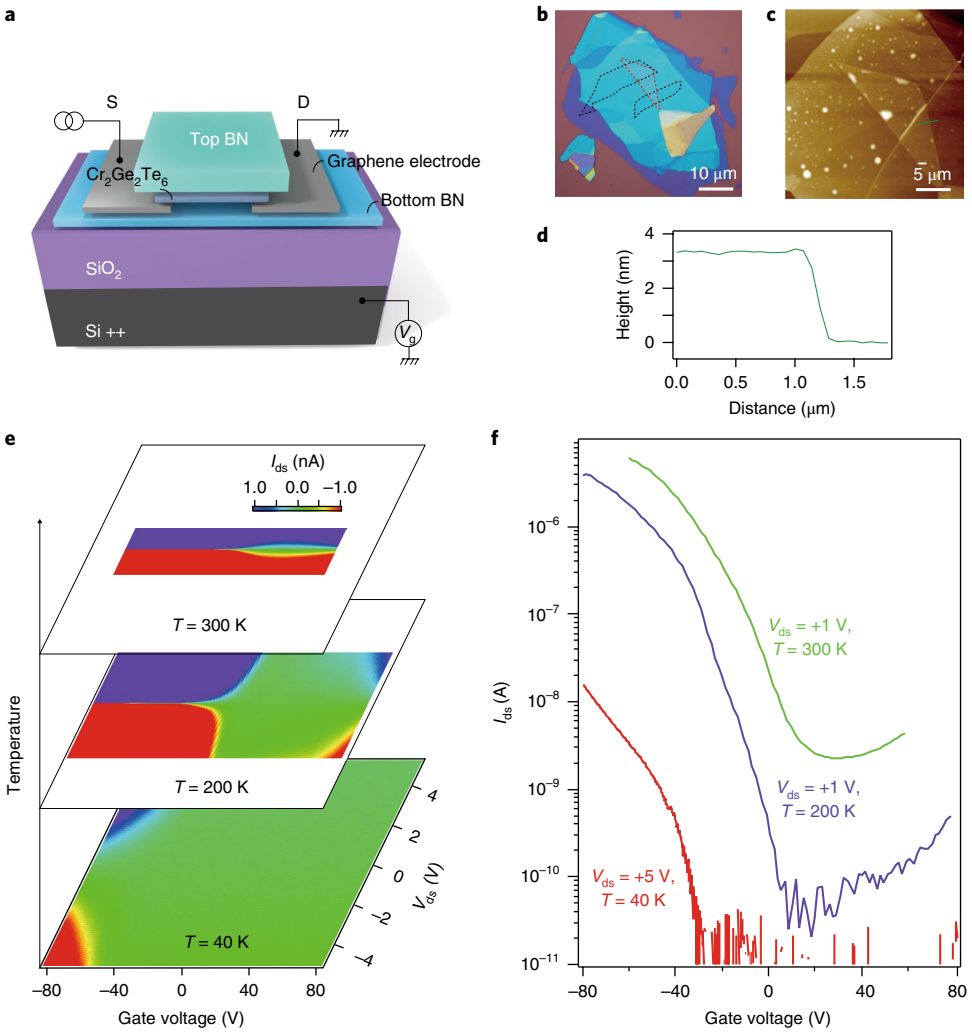

Fig. 3 | Electrical transport properties of BN-encapsulated few-layered $Cr_2Ge_2Te_6$ FETs with Si gate. a, Schematic of a few-layered $Cr_2Ge_2Te_6$ flake encapsulated by two h-BN layers, contacted via graphene electrodes. **b**,**c**, Optical and AFM images of the sample; black and red dashed lines indicate graphene electrodes and $Cr_2Ge_2Te_6$ flake, respectively. **d**, Height profile of the $Cr_2Ge_2Te_6$ flake along the solid green line in **c**. **e**, Colour map of *I*–*V* curves as a function of gate voltage at different temperatures. The colour code of I_{ds} is set with a threshold of ±1 nA to show the gapped regions below 1 nA. **f**, Field-effect curves with different V_{ds} and temperatures, measured in the same sample.

concentration) could only be estimated using a calibrated value reported elsewhere, which is a rather qualitative estimation. With the 3.5 nm $Cr_2Ge_2Te_6$ and a Si gate, we were able to quantify the carrier concentrations induced by the gate. As shown in Supplementary Fig. 18, H_s and M_s could be extracted at different doping levels. Bipolar gate tunability of the magnetization loop is seen, with a stronger gating effect on the electron side. Interestingly, a gapped region where the doping effects are negligible can be observed in the range of $V_g \sim -30$ and 0 V. Note that, in electrical transport, this gate range is turned into an off state, as seen in the field-effect curve. However, this might be due to a non-ohmic contact. In the optical measurements, the doping effects can be more intrinsic, which excludes external parasitic effects such as contact issues.

Furthermore, by monitoring the Kerr signal with a saturation field such as 200 mT while varying the temperature, we were able to measure the Curie temperature at different doping levels, as shown in Supplementary Fig. 19. A phase diagram of the magnetization in the parameter space of the gate voltage and temperature is shown in Supplementary Fig. 19b. Here, within the detection precision, no obvious gating effects were seen on T_C, indicating a rather constant exchange coupling stiffness J in the ferromagnet. More discussion will be given in the following paragraphs.

We now compare the measured data with first-principles calculations and micromagnetic simulations. Given that our experimental $Cr_2Ge_2Te_6$ flakes are more than 18 nm (Figs. 1 and 2) and around 3–4 nm (Figs. 3 and 4) in thicknesses, we use three-layer bulk and six-layer slab phases of $Cr_2Ge_2Te_6$ to represent the two structures for computational simplicity. In Fig. 5a,b we show the electronic band structure and density of states (DOS) of a few-layered $Cr_2Ge_2Te_6$ flake (six-layer slab). Few-layered $Cr_2Ge_2Te_6$ is a ferromagnetic semiconductor, and both spin majority and minority (spin up and down) bands are mainly contributed by the *p* orbital of Te atoms in the vicinity of the valence band maximum (VBM) and by the *d* orbitals of Cr atoms near the conduction band minimum (CBM), as seen from the projected DOS in Supplementary Fig. 20. Hole (electron) doping by electrostatic gating will shift the Fermi level into the valence (conduction) band by depleting (filling) Te-*p* (Cr-*d*) orbitals. It is worth pointing out that the bands near the VBM and CBM are contributed by spin minority and spin majority states, respectively, in a narrow energy range, suggesting that an increased net magnetic moment M_s will be anticipated for mild doping of either electrons or holes, as indicated in the schematic in Fig. 5c. Indeed, the doping-enhanced M_s has been observed with carrier concentrations below 1×10^{13} cm^{-2} in our experiment, as shown in Fig. 4c,d and

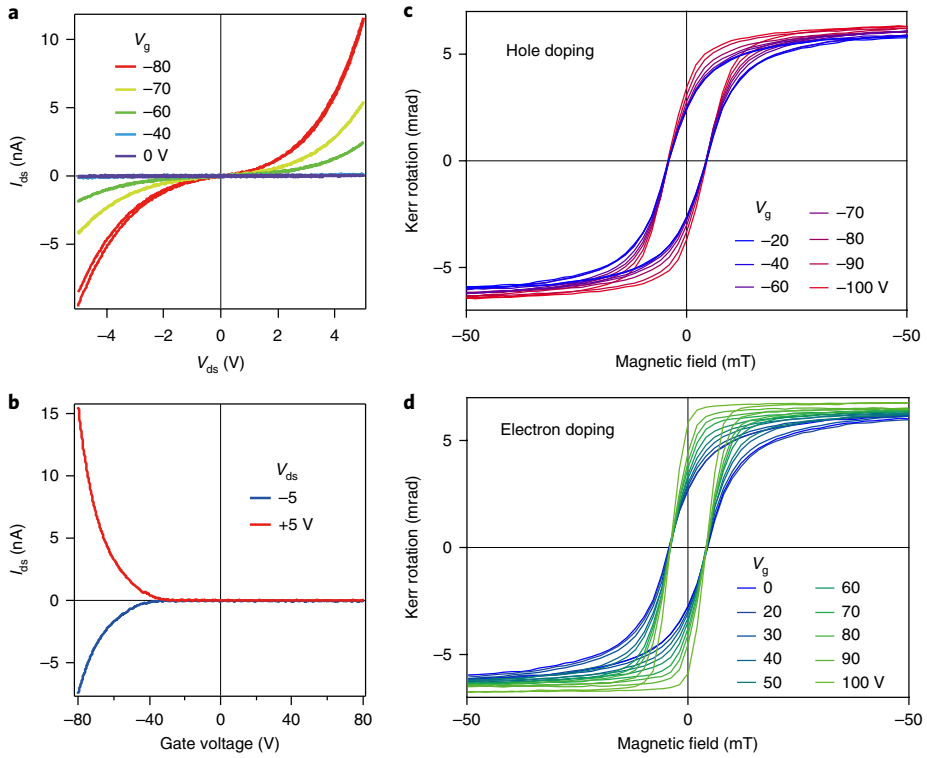

Fig. 4 | Kerr measurement of BN-encapsulated 3.5 nm $Cr_2Ge_2Te_6$ sample with solid Si gate. a, *I*–*V* characteristics of the same device with five different fixed Si gate voltages measured at 40 K. **b**, Field-effect curves at 40 K with $V_{ds} = -5$ and +5 V (blue and red, respectively). **c**,**d**, Kerr angle measured at 40 K for negative (**c**) and positive (**d**) gate voltages respectively.

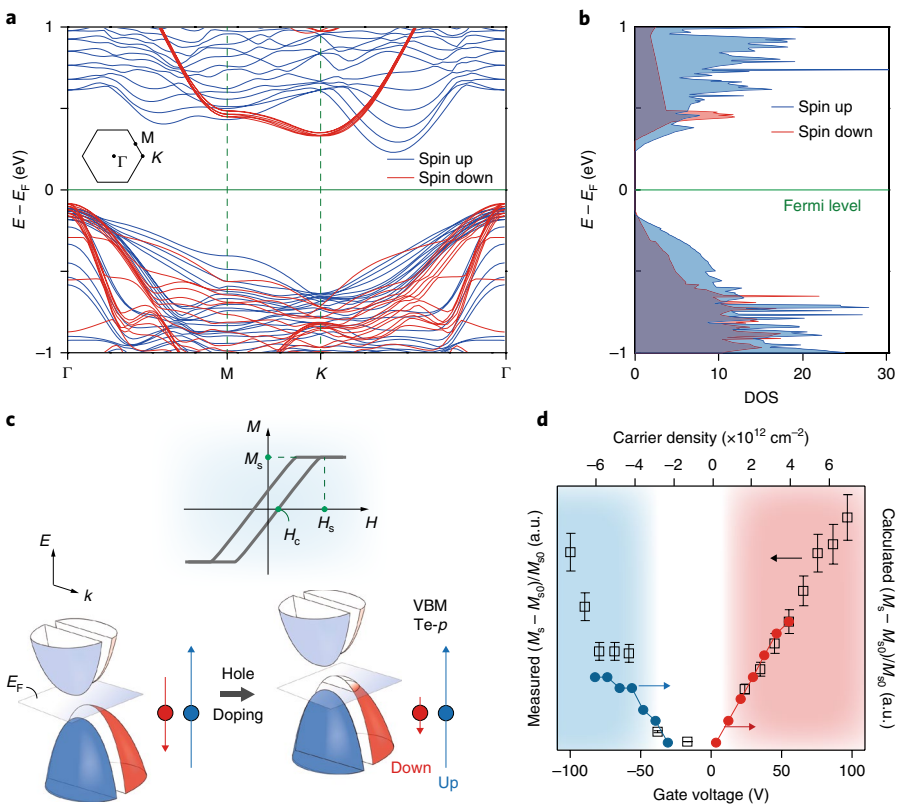

Fig. 5 | First-principles simulations. a, Spin-polarized band structure of few-layered $Cr_2Ge_2Te_6$. **b**, Calculated electron DOS. **c**, Top, schematic magnetization reversal loop. Bottom, schematic of the spin realignment model via Fermi level shifting during electrostatic doping. Red and blue represent down spins from Te atoms and up spins from Cr atoms, respectively. Semi-transparent and solid colours are empty and occupied bands, respectively. **d**, Blue and red solid circles with solid lines are the simulated evolution of normalized spin magnetization $(M_s - M_{s0})/M_{s0}$ (M_{s0} is the M_s at the band edge) as a function of hole and electron carrier density, respectively. Black open squares show the same experimental data as given in Supplementary Fig. 18.

summarized in Fig. 5d. In Fig. 5d, normalized spin magnetization as a function of carrier density is compared between the experiment (black open squares) and first-principles calculations (red and blue filled circles), with good agreement. Obviously, bipolar gate enhancement of the magnetization in the 2D limit is achieved. Electron doping seems to be advantageous over hole doping in terms of the rate of increase of M_s, which is ascribed to the subtle orbital character of the CBM and VBM (the *d* orbital for the CBM due to the Cr atoms gives rise to a potentially larger magnetization than the *p* orbital for the VBM from Te atoms; Supplementary Fig. 20).

To understand the coercivity field H_c and saturation field H_s as a function of electrostatic doping, we performed micromagnetic simulations to study multiple-domain properties. All the parameters in the Heisenberg model, such as exchange stiffness *J*, magneto-crystalline anisotropy energy *D* and saturation magnetization M_s, are chosen based on our density functional calculations. These calculations show that, with increasing carrier concentration, the magnitude of *J* increases while *D* decreases, as shown in Supplementary Fig. 21. A small variation (~0.5%) in the calculated exchange stiffness *J* with carrier density within the experimental range explains why the Curie temperature T_C ($T_C \sim J$ according to the Weiss–Heisenberg model[27]) does not change much, as indicated in Supplementary Fig. 19b. Incorporating *J* and *D* into the model, we solve for hysteresis loops at different (*J*, *D*) pairs (Supplementary Fig. 22). The phenomenon observed in Fig. 4, where the H_c of few-layered $Cr_2Ge_2Te_6$ is almost insensitive to doping but H_s changes inversely with doping, can be reproduced well by our simulations, as shown in Supplementary Fig. 22.

To conclude, we have demonstrated that few-layered semiconducting $Cr_2Ge_2Te_6$ devices can serve as transistors that exhibit a gate-tuned modification of magnetism, as observed from micro-area Kerr measurements below the ferromagnetic Curie temperature via gating. The observed behaviour of bipolar gate-tuned magnetism in few-layered $Cr_2Ge_2Te_6$ may be attributed to a rebalance of the spin-polarized band structure while tuning its Fermi level. Our findings therefore indicate that vdW magnets can form a promising platform that may open further opportunities for future applications in spin transistors.

Note added in proof. During consideration of our work, three papers showing gate-tuning effects in 2D antiferromagnetic CrI_3, as well as in 2D metallic Fe_3GeTe_2, were published[28–30].

Methods

Methods, including statements of data availability and any associated accession codes and references, are available at https://doi.org/10.1038/s41565-018-0186-z.

Received: 22 February 2018; Accepted: 5 June 2018;
Published online: 2 July 2018

References

1. Chappert, C., Fert, A. & Nguyen Van Dau, F. The emergence of spin electronics in data storage. *Nat. Mater.* **6**, 813–823 (2007).
2. Matsukura, F., Tokura, Y. & Ohno, H. Control of magnetism by electric fields. *Nat. Nanotech.* **10**, 209–220 (2015).
3. Lin, M.W. et al. Ultrathin nanosheets of $CrSiTe_3$: a semiconducting two-dimensional ferromagnetic material. *J. Mater. Chem. C* **4**, 315–322 (2016).
4. Xing, W. et al. Electric field effect in multilayer $Cr_2Ge_2Te_6$: a ferromagnetic 2D material. *2D Mater.* **4**, 024009 (2017).
5. Huang, B. et al. Layer-dependent ferromagnetism in a van der Waals crystal down to the monolayer limit. *Nature* **546**, 270–273 (2017).
6. Gong, C. et al. Discovery of intrinsic ferromagnetism in two-dimensional van der Waals crystals. *Nature* **546**, 265–269 (2017).
7. Wang, Z. et al. Very large tunneling magnetoresistance in layered magnetic semiconductor CrI_3. Preprint at https://arxiv.org/abs/1801.08188 (2018).
8. Klein, D. R. et al. Probing magnetism in 2D van der Waals crystalline insulators via electron tunneling. *Science* **360**, 1218–1222 (2018).
9. Song, T. C. et al. Giant tunneling magnetoresistance in spin-filter van der Waals heterostructures. *Science* **360**, 1214–1218 (2018).
10. Sivadas, N., Daniels, M. W., Swendsen, R. H., Okamoto, S. & Xiao, D. Magnetic ground state of semiconducting transition-metal trichalcogenide monolayers. *Phys. Rev. B* **91**, 235425 (2015).
11. Mounet, N. et al. Two-dimensional materials from high-throughput computational exfoliation ofexperimentally known compounds. *Nat. Nanotech.* **13**, 246–252 (2018).
12. Bonilla, M. et al. Strong room-temperature ferromagnetism in VSe_2 monolayers on van der Waals substrates. *Nat. Nanotech.* **13**, 289–293 (2018).
13. Arai, M. et al. Construction of van der Waals magnetic tunnel junction using ferromagnetic layereddichalcogenide. *Appl. Phys. Lett.* **107**, 103107 (2015).
14. Cherifi, R. O. et al. Electric-field control of magnetic order above room temperature. *Nat. Mater.* **13**, 345–351 (2014).
15. Chiba, D. et al. Electrical control of the ferromagnetic phase transition in cobalt at room temperature. *Nat. Mater.* **10**, 853–856 (2011).
16. Weisheit, M. Electric Field-induced modification of magnetism in thin-film ferromagnets. *Science* **315**, 349–351 (2007).
17. Shimamura, K. et al. Electrical control of Curie temperature in cobalt using an ionic liquid film. *Appl. Phys. Lett.* **100**, 122402 (2012).
18. Wang, W. G., Li, M., Hageman, S. & Chien, C. L. Electric-field-assisted switching in magnetic tunneljunctions. *Nat. Mater.* **11**, 64–68 (2012).
19. Maruyama, T. et al. Large voltage-induced magnetic anisotropy change in a few atomic layers of iron. *Nat. Nanotech.* **4**, 158–161 (2009).
20. Wang, Y. Y. et al. Electrical control of the exchange spring in antiferromagnetic metals. *Adv. Mater.* **27**, 3196–3201 (2015).
21. Ohno, H. et al. Electric-field control of ferromagnetism. *Nature* **408**, 944–946 (2000).
22. Chiba, D., Yamanouchi, M., Matsukura, F. & Ohno, H. Electrical manipulation of magnetization reversal in aferromagnetic semiconductor. *Science* **301**, 943–945 (2003).
23. Zhang, Y. B., Tan, Y. W., Stormer, H. L. & Kim, P. Experimental observation of the quantum Hall effect and Berry's phase in graphene. *Nature* **438**, 201–204 (2005).
24. Ye, J. T. et al. Liquid-gated interface superconductivity on an atomically flat film. *Nat. Mater.* **9**, 125–128 (2010).
25. Yuan, H. T. et al. Electrostatic and electrochemical nature of liquid-gated electric-double-layer transistorsbased on oxide semiconductors. *J. Am. Chem. Soc.* **132**, 18402–18407 (2010).
26. Guo, T. et al. Multiple structure and symmetry types in narrow temperature and magnetic field ranges intwo-dimensional $Cr_2Ge_2Te_6$ crystal. Preprint at https://arxiv.org/abs/1803.06113 (2018).
27. Stöhr, J. & Siegmann, H. C. *Magnetism from Fundamentals to Nanoscale Dynamics* (Springer, Berlin, 2006).
28. Jiang, S. W., Li, L. Z., Wang, Z. F., Mak, K. F. & Shan, J. Controlling magnetism in 2D CrI_3 by electrostatic doping. *Nat. Nanotech.* https://doi.org/10.1038/s41565-018-0135-x (2018).
29. Huang, B. et al. Electrical control of 2D magnetism in bilayer CrI_3. *Nat. Nanotech.* https://doi.org/10.1038/s41565-018-0121-3.
30. Deng, Y. J. et al. Gate-tunable room-temperature ferromagnetism in two-dimensional Fe_3GeTe_2. Preprint at https://arxiv.org/abs/1803.02038 (2018).

Acknowledgements

This work was supported by the National Key R&D Program of China (2017YFA0206302) and by the National Natural Science Foundation of China (NSFC; grants 11504385 and 51627801). Z.Z. acknowledges support from the NSFC (grant 51331006) and the CAS (project KJZD-EW-M05-3). T.Y. acknowledges support from the Major Program of Aerospace Advanced Manufacturing Technology Research Foundation, NSFC and CASC (grant U1537204). The work in Shanxi University was supported financially by the NSFC (grant 61574087) and the Fund for Shanxi '1331 Project' Key Subjects Construction (1331KSC). D.S. acknowledges support from the NSFC (grants 51272256, 61422406 and 61574143) and MSTC (grant 2016YFB04001100). S.O. acknowledges support from Grants-in-Aid for Scientific Research (S) (25220604) and LANEF. The authors are grateful for discussions with H. Yuan.

Author contributions

Z.H. and Z.Z. conceived the experiment and supervised the overall project. Z.W., X.L. and Y.Y. fabricated the samples. Z.W., T.Z., Ya.L., Y.C. and Z.H. carried out experimental measurements. S.O. provided the ionic liquid and advised on the experiment. B.D., J.H. and T.Y. conducted the theoretical simulations. Z.H., M.D., T.Z., T.Y. and Y.C. analysed the data. The manuscript was written by Z.H., Y.C. and T.Y. All authors discussed the results and commented on the manuscript.

Competing interests

The authors declare no competing interests.

Additional information

Supplementary information is available for this paper at https://doi.org/10.1038/s41565-018-0186-z.

Reprints and permissions information is available at www.nature.com/reprints.

Correspondence and requests for materials should be addressed to Y.C. or T.Y. or Z.H.

Publisher's note: Springer Nature remains neutral with regard to jurisdictional claims in published maps and institutional affiliations.

Methods

Single-crystal $Cr_2Ge_2Te_6$ was prepared via the Te self-flux method. Raw material powders with a stoichiometric ratio of Cr (purity 99.9%):Ge (purity 99.9%):Te (purity 99.99%) = 1:4:20 were mixed and kept at 950 °C for 6 h. The mixture was then cooled at a rate of 2 °C h^{-1}, followed by centrifugation at 500 °C. For devices studied in air we applied the scotch tape method to exfoliate the bulk and deposited few-layered $Cr_2Ge_2Te_6$ onto 285-nm-thick silicon oxide grown on heavily doped silicon wafers for further FET fabrication. Few-layered $Cr_2Ge_2Te_6$ devices encapsulated by h-BN (crystals from HQ-Graphene) were fabricated in a glove box. Sample morphology was characterized using a Bruker-Icon AFM system.

Kerr rotation was performed to monitor the electrically tunable out-of-plane magnetization of the sample. A continuous-wave Ti:sapphire laser with 100 kHz bandwidth was used to generate linearly polarized light, and the probe energy was fixed at 1.550 eV for all measurements. By using a lens with a numerical aperture of 0.50, the Gaussian beam was tightly focused with a sigma width of 2 μm on the sample surface. A balanced photodiode bridge was adopted to sensitively monitor the polarization change of the probe beam due to the polar magneto-optic Kerr effect (MOKE). The sample was mounted in the Faraday geometry in a helium-free cryostat; that is, both the external applied magnetic field B_{ext} and the light propagation vector were along the out-of-plane direction of the sample. The sample was moved by an x–y–z piezo stage with an accuracy of 200 nm, and the sample temperature could be set from 4.0 K to 350 K. To characterize the coercive field and saturation magnetization of the sample, MOKE loop measurements were performed continuously by scanning the longitudinal magnetic field from a negative $|B_{ext}|$ to a positive $|B_{ext}|$, and backwards to $-|B_{ext}|$, which produced the MOKE loops recorded under various experiment conditions.

The simulations in this work were partly carried out by using first-principles density functional theory as implemented in the VASP code[31] at the local spin density approximation (LSDA) plus U level[32]. A Coulomb repulsion U (0.8 eV) was considered (Supplementary Fig. 23)[6]. Projector augmented wave (PAW) pseudopotentials[33] were used to describe electron–ion interactions. The Brillouin zone of the primitive unit cell was sampled by $6\times6\times1$ k-points for layered $Cr_2Ge_2Te_6$. We adopted 500 eV as the electronic kinetic energy cutoff for the plane-wave basis and 1×10^{-8} eV as the criterion for reaching self-consistency. The magneto-crystalline anisotropy energy was calculated by using a more dense k-mesh, that is, $13\times13\times1$ k-points. Micromagnetics simulations were performed by using an atomistic spin model based on the Heisenberg Hamiltonian as implemented in the Vampire software package[34]. The lattice parameters were drawn from the Rietveld refinement of our X-ray diffraction data, and the parameters of the bulk phase were consistent with those of the Springer Materials database.

Data availability. The data sets generated during and/or analysed during the current study are available from the corresponding authors upon reasonable request.

References

31. Kresse, G. & Furthmüller, J. Efficient iterative schemes for *ab initio* total-energy calculations using a planewavebasis set. *Phys. Rev. B.* **54**, 11169 (1996).
32. Cococcioni, M. & de Gironcoli, S. Linear response approach to the calculation of the effective interactionparameters in the LDA+U method. *Phys. Rev. B.* **71**, 035105 (2005).
33. Kresse, G. & Joubert, D. From ultrasoft pseudopotentials to the projector augmented-wave method. *Phys. Rev. B* **59**, 1758 (1999).
34. Evans, R. F. L. et al. Atomistic spin model simulations of magnetic nanomaterials. *J. Phys. Condens. Matter* **26**, 103202 (2014).